INTERNATIONAL JOURNAL FOR NUMERICAL METHODS IN FLUIDS
Int. J. Numer. Meth. Fluids **29**: 1–18 (1999)

DIE SWELL MEASUREMENTS OF SECOND-ORDER FLUIDS: NUMERICAL EXPERIMENTS

LUIS GAST*,[1] AND WILLIAM ELLINGSON

Energy Technology Division, Argonne National Laboratory, Argonne, Argonne 60437, IL, USA

SUMMARY

An analysis of the flow of a second-order fluid is presented. Reference values for some variables are defined, and with these a non-dimensional formulation of the governing equations. From this formulation, three dimensionless numbers appear; one is the Reynolds number, and two numbers that are called the first- and second-dimensionless normal stress (NSD) coefficients. The equations of motion are solved by a finite element method using a commercially available program (Fidap), and the steady state converged solution was used to measure the die swell. The factors that influence die swell and that are studied in this work include: the die geometry for circular cross sectional dies, including tubular, converging, diverging, half-converging/half-tubular shapes; fluid characteristics such as Reynolds number and first- and second-DNS coefficients (both positive and negative values); and flow rates, as determined by the maximum velocity in a parabolic velocity profile at the entrance to the die. The results suggest that shear and deformation histories of the fluid directly influence not only swell characteristics, but also convergence characteristics of the numerical simulation. Copyright © 1999 John Wiley & Sons, Ltd.

KEY WORDS: die swell; second-order fluid; finite element

1. INTRODUCTION

Many liquids of industrial, geological and natural fields cannot be adequately described by the classical linear viscous fluid model. Many models have been suggested to explain the departure from the Newtonian behavior. One such family of models is referred to as *fluids of differential type*, a subset of which are the incompressible fluids of grade 2, also known as second-order fluids or Rivlin–Ericksen fluids. Fluids of this type cannot experience stress relaxation, but can adequately represent other types of flow which will be discussed later on in the paper. Free-surface flows are also of practical interest. One of the most common examples is the flow of material as it emerges from a circular die. It is well-known that for a Newtonian liquid, the diameter of the issuing liquid (the extrudate) will be slightly larger or slightly smaller than that of the die orifice, depending on the Reynolds number; this indicates that viscous effects contribute to the swelling mechanism. For other materials, the ratio of the diameter of the jet to the diameter of the die orifice (called B) can be significantly greater than unity, a phenomenon commonly known as die swell.

The diameter of the extrudate has a direct influence on the final product being produced. Thus, it is desirable to be able to identify and qualify the conditions that would generate maximum swell, as well as to predict its magnitude for a particular material being modeled.

* Correspondence to: Robert Morris College, 180 N. Lasalle St., Chicago 60601, IL, USA.
[1] Current address: Robert Morris College, 180 N. Lasalle St., Chicago 60601, IL, USA.

CCC 0271–2091/99/010001–18$17.50

Received 18 November 1996
Revised 13 August 1997

The two factors that determine die swell are the process conditions and the properties of the fluid. Process conditions include the geometry of the die (a circular cross section has been assumed in all cases), mass flow rate, and temperature. Fluid properties include the viscosity, density, and first and the normal stress coefficients. The purpose of this paper is to establish some qualitative trends of the die swell produced by changes in the process conditions and the properties of the fluid.

2. FUNDAMENTAL EQUATIONS

It is instructive to write down the equations governing the motion of the fluid. An asterix (*) indicates a quantity with physical dimensions. In a later section, non-dimensionalized equations are presented and results are given in terms of non-dimensional quantities.

Let x_i^* be the ith component of the particle position vector, $\mathbf{x}$. In the case of an incompressible fluid, and neglecting body forces, the equations [1] that must be solved are the equation of mass conservation,

$$\frac{\partial u_1^*}{\partial x_1^*} + \frac{\partial u_2^*}{\partial x_2^*} + \frac{\partial u_3^*}{\partial x_3^*} = 0, \tag{1}$$

where u_i^* is the ith component of the velocity vector, $\mathbf{v}$; the equation of angular momentum conservation,

$$\sigma_{ij}^* = \sigma_{ji}^*, \tag{2}$$

where σ_{ij} is the stress tensor; and the equation of linear momentum conservation,

$$\rho^*\left(\frac{\partial u_i^*}{\partial t^*} + u_j^* u_{i,j}^*\right) = \frac{\partial \sigma_{ij}^*}{\partial x_j^*}, \tag{3}$$

where ρ^* represents density.

Consider the isothermal case, in which there is no need to include the energy equation. The fundamental problem in rheology is that in the linear momentum equation (Equation (3) above), an expression is needed for the stress tensor in terms of the kinematic tensors. This expression is what is commonly known as the 'constitutive equation' for stress and is discussed in the next section.

3. CONSTITUTIVE EQUATION

In a fluid at rest, $\sigma_{ij}^* = -p^*\delta_{ij}$, where p is the pressure and δ_{ij} is the unit tensor. For a fluid in motion, and for a 'second-order' fluid model, the extra stress tensor $\sigma_{ij}^* + p^*\delta_{ij}$ can be represented by

$$\sigma^* + p^*\mathbf{I} = \eta^*\mathbf{A}_1^* + [v_1^*(0) + v_2^*(0)](\mathbf{A}_1^*)^2 - \frac{1}{2}v_1^*(0)\mathbf{A}_2^*, \tag{4}$$

where $\mathbf{I} = \delta_{ij}$ is the unit tensor, $\mathbf{A}_1^*$ $[= (A_{ij}^{(1)})^*\}$ and $\mathbf{A}_2^*$ $[= (A_{ij}^{(2)})^*\}$ are the first and second Rivlin–Ericksen tensors, η^* is the Newtonian viscosity, and v_1^* and v_2^* are the first and second normal stress coefficients. These stress coefficients are a function of the shear rate $\dot{\gamma}^*$, i.e. $v^* = v^*(\dot{\gamma}^*)$, and can be determined by viscometric measurements.

The equation of linear momentum can be combined into a single expression by using Equations (3) and (4). In tensor notation, this would be,

$$\rho^*\left(\frac{\partial u_i^*}{\partial t^*} + u_l^* u_{i,j}^*\right) = -\frac{\partial p^*}{\partial x_j^*}\delta_{ij} + \eta^*\frac{\partial (A_{ij}^{(1)})^*}{\partial x_j^*} + [v_1^*(0) + v_2^*(0)]\frac{\partial}{\partial x_j^*}[(A_{ij}^{(1)})^*]^2 - \frac{1}{2}v_1^*(0)\frac{\partial}{\partial x_j^*}(A_{ij}^{(2)})^*. \quad (5)$$

4. THE SECOND-ORDER FLUID MODEL

A grade 2 fluid model, like all flows, will be shaped and formed by its boundary conditions. This model can also incorporate a mechanism for dissipation similar to that of the Newtonian fluid model, but it further allows for non-zero normal stress differences, two material parameters, and provides for a new mechanism for diffusion of velocity and vorticity. On this account, this model opens up new possibilities and introduces a richer physics that is not available with the Newtonian model. Similar to the Newtonian fluid model, it also has a frame-indifferent constitutive equation. It is mainly for these reasons that this model deserves studying. As for its limitation, this model cannot describe materials that experience stress relaxation.

The formula of Equation (4) was first obtained by Criminale *et al*. [2], who showed that with η^*, and v_1^* and v_2^* possibly depending on $\dot{\gamma}^*$, this equation will give the stress exactly in any fluid of differential type, undergoing steady, viscometric flows. Coleman and Noll [3] further showed that Equation (4) also emerged as a second-order *retardation* expansion of the stress, where the first-order of this *retardation* would be the Navier–Stokes form of the stress. Previous applications of this model have been discussed by Truesdell and Noll [4].

In the past, however, this fluid flow model has generated a lot of controversy. Two of the most polemical points are, the rest-state would seem to be unstable (Joseph [5,6]), and a given sign of the first and/or second normal stress coefficients v_1^* and v_2^* would seem to be associated with unstable behavior (Ting [7]; Markovitz and Brown [8]; Colemann and Markovitz [9]; Coleman *et al*. [10]; Dunn and Fosdick [11]). A thermodynamic analysis of these two points is presented by Dunn and Rajagopal [12], including some historical background and development of flows of differential type. Results and analysis of the rest-state is beyond the scope of this work, but it suffices to say that Dunn and Rajagopal have proven that, fluids that are consistent with thermodynamics, are well behaved in this limit. This paper is limited to the analysis of such fluids. In a following section, the issue pertaining to the sign of the normal stress coefficients will be discussed in more depth. At this point it can be anticipated that solutions were found for both positive and negative normal stress coefficient values.

5. DIMENSIONLESS FORM OF THE EQUATIONS

In order to express Equation (5) in a non-dimensional form, the following characteristic quantities measured at the die exit were used (see Figure 1); V_0^* is a reference value of the velocity, and L_0^* is the distance corresponding to the half-radius of the die. With these values, we can define the following dimensionless quantities

$$x=\frac{x^*}{L_0^*},\quad u=\frac{u^*}{V_0^*},\quad t=\frac{t^*V_0^*}{L_0^*},\quad p=\frac{p^*}{\rho^*(V_0^*)^2},\quad A_{ij}^{(1)}=\frac{(A_{ij}^{(1)})^*L_0^*}{V_0^*},\quad A_{ij}^{(2)}=\frac{(A_{ij}^{(2)})^*(L_0^*)^2}{(V_0^*)^2}. \tag{6}$$

If these values are replaced in Equation (5), the term on the left-hand side is now

$$\frac{\rho^*(V_0^*)^2}{L_0^*}\left(\frac{\partial u_i}{\partial t}+u_i u_{i,j}\right). \tag{7}$$

The term on the right-hand side of Equation (5) is now

$$-\frac{\rho^*(V_0^*)^2}{L_0^*}\frac{\partial p}{\partial x_j}\delta_{ij}+\frac{\eta^*V_0^*}{(L_0^*)^2}\frac{\partial A_{ij}^{(1)}}{\partial x_j}+[v_1^*(0)+v_2^*(0)]\frac{(V_0^*)^2}{(L_0^*)^3}\frac{\partial}{\partial x_j}(A_{ij}^{(1)})^2-\frac{1}{2}v_1^*(0)\frac{(V_0^*)^2}{(L_0^*)^3}\frac{\partial A_{ij}^{(2)}}{\partial x_j}. \tag{8}$$

Multiplying both Equations (7) and (8) by $[(\rho^*(V_0^*)^2)/L_0^*]^{-1}$, the final form of the equation of conservation of linear momentum is obtained

$$\left(\frac{\partial u_i}{\partial t}+u_i u_{i,j}\right)=-\frac{\partial p}{\partial x_j}\delta_{ij}+\frac{\eta^*}{\rho^*V_0^*L_0^*}\frac{\partial A_{ij}^{(1)}}{\partial x_j}+\frac{v_1^*(0)+v_2^*(0)}{\rho^*(L_0^*)^2}\frac{\partial}{\partial x_j}(A_{ij}^{(1)})^2-\frac{1}{2}\frac{v_1^*(0)}{\rho^*(L_0^*)}\frac{\partial A_{ij}^{(2)}}{\partial x_j}. \tag{9}$$

Equation (9) presents three dimensionless numbers that characterize flows of second-order fluids. One is

$$\left(\frac{\eta^*}{\rho^*V_0^*L_0^*}\right)=\frac{1}{Re}, \tag{10}$$

or the inverse of the Reynolds number. The other two dimensionless numbers are

$$\left[\frac{v_1^*}{\rho^*(L_0^*)^2}\right]\quad\text{and}\quad\left[\frac{v_2^*}{\rho^*(L_0^*)^2}\right], \tag{11}$$

and to the knowledge of the authors, these have not been given any name in any prior work. Let us call these NSD_1 and NSD_2, for normal stress dimensionless numbers 1 and 2. The NSD number might be perceived as a ratio of the normal forces to inertial forces. This can be seen by expressing it as

$$\frac{v^*}{\rho^*(L_0^*)^2}=\frac{v^*\left(\frac{V_0^*}{L_0^*}\right)}{\rho^*V_0^*L_0^*}.$$

The quantity (V_0^*/L_0^*), which was multiplied in the numerator and denominator of the NSD number, represents the shear rate at the wall. The numerator consists of the normal stress coefficient multiplied by shear rate (an indication of the normal stress produced by the

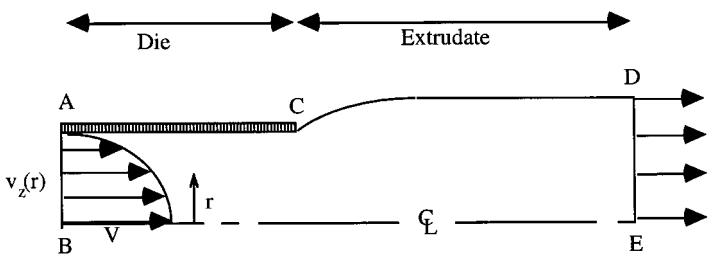

Figure 1. Boundary conditions for the die swell problem.

shearing). The denominator consists of a quantity that represents the inertial stress (analogous to the similar interpretation given for the same term in the Reynolds number). However, it should be noted that the NSD numbers do not depend on velocity.

In terms of these dimensionless numbers, Equation (9) can be written as

$$\left(\frac{\partial u_i}{\partial t}+u_i u_{i,j}\right)=-\frac{\partial p}{\partial x_j}\delta_{ij}+\frac{1}{Re}\frac{\partial A_{ij}^{(1)}}{\partial x_j}+\left\{(\mathrm{NSD}_1+\mathrm{NSD}_2)\frac{\partial}{\partial x_j}(A_{ij}^{(1)})^2-\frac{1}{2}\mathrm{NSD}_1\frac{\partial A_{ij}^{(2)}}{\partial x_j}\right\}. \tag{12}$$

All results presented here are based on the above dimensionless formulation of the equations.

6. BOUNDARY CONDITIONS

Boundary conditions present a difficult issue on flows of this nature. There are special flow situations which require very special boundary conditions. In general, the boundary conditions used in the solution of the Navier–Stokes equations (in terms of velocity and pressure fields only) are not sufficient to completely render the problem determinate. There is no complete mathematical theory, to the knowledge of the authors, that would help in the selection. On the other hand, Equation (3) would indicate that the necessary boundary conditions are velocity and the stress fields specified at all boundaries. This is however, not necessary in the present case, as velocity fields will often place conditions on stress. The conditions needed are described next, in a way not different from other researchers who have worked on similar problems, some of them on viscoelastic materials; see e.g. Keunings [13]; Barakos and Mitsoulis [14]; Young-Cheol and Ryan [15]; Giorgious *et al.* [16]; and Hurez *et al.* [17].

The kinematic equation of motion to be solved is that of Equation (12), where all boundary conditions make reference to Figure 1.

6.1. At the die entrance AB

We assume a fully developed flow, and the velocity follows a parabolic distribution, i.e. on AB,

$$v_z^*(r)=V_{\max}^*[1-(r^*/L_0^*)^2] \quad \text{and} \quad v_r^*=v_\theta^*=0, \tag{13}$$

where θ represents the azimuth angle, $V_{\max}^*$ is the velocity at the center line of the die, and $2L_0^*$ is the diameter of the die. Rewriting in terms of dimensionless parameters,

$$v_z(r)=V(1-r^2) \quad \text{and} \quad v_r=v_\theta=0, \tag{14}$$

where $r=r^*/L_0^*$, $v=v^*/V_0^*$ and $V=V_{\max}^*/V_0^*$.

This parabolic velocity distribution would correspond to the solution of the Newtonian flow. This velocity distribution would satisfy the equations of a second-order flow model only in the case of creeping (non-inertial) flow [18–20]. When inertial effects are included there is no analogy. This velocity distribution, however, was used in all cases, and was specified at a distance $3.5L_0^*$ upstream from the die exit ($3L_0^*$ was specified in a converging-tubular die geometry). The hypothesis was that any deviation from the parabolic profile in an actual run should adjust to a new steady state condition before reaching the die exit.

This hypothesis was tested by extending the upstream length of the tube to $10L_0^*$ and observing the change in velocity profiles along the tube for a typical set of values. The results

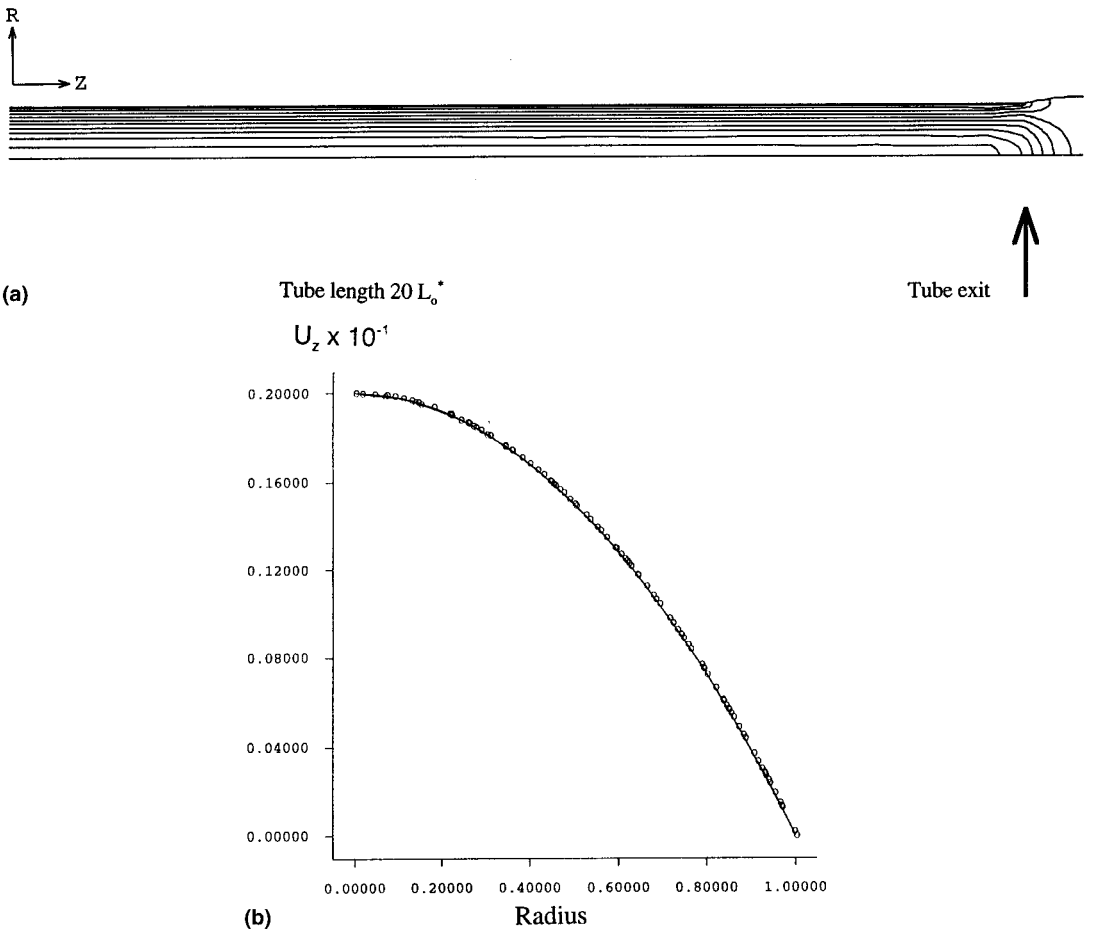

Figure 2. (a) Streamlines upstream from die exit. (b) Radial velocity distribution from tube entrance at 0, 5, 10 and $15L_0^*$. (c) U_z vs. axial distance: top graph, radius $0.5L_0^*$; bottom graph, radius 0, die exit at $z = 0$, flow in tube $-20L_0^*$ to $z = 0$, free flow $z = 0$–$20L_0^*$.

are presented in Figure 2. (The particular details of the simulation will be explained in a later section. Note also the flow at the tube exit, including the swell of the material as it comes out). It can be observed that the velocity profile does not change for all practical purposes, along the length of the tube. All graphs illustrate the fact that noticeable velocity changes take place at the die exit. It is then concluded that this parabolic velocity is an acceptable boundary condition at the entrance plane, and further more, that $3.5L_0^*$ provides an adequate distance for the flow to reach a steady flow condition before the die exit. This statement should not be confused with the possibility of fluid 'conditioning' before the die exit. The prior history of the flow is going to affect the die swell as will be observed later.

6.2. On AC or the die wall

There is no slip present on the wall, i.e.

$$v_z^* = v_r^* = v_\theta^* = 0, \quad \text{or} \quad v_z = v_r = v_\theta = 0.$$

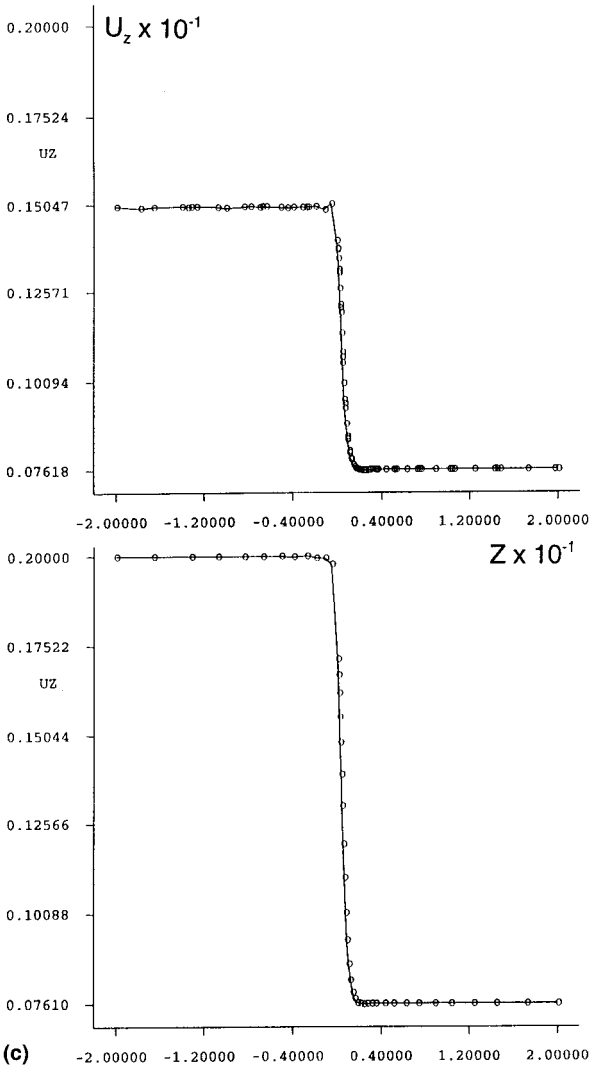

Figure 2 (*Continued*)

6.3. On CD is a free-surface

We specify both a velocity and a stress boundary condition. These are,

$v_n^* = 0$ or $v_n = 0$ (velocity normal to the surface),

σ_{nn}^* and $\sigma_{ns}^* = 0$ or σ_{nn} and $\sigma_{ns} = 0$ (normal and tangential shear stress),

$\sigma_{n\theta}^*$ and $\sigma_{\theta s}^* = 0$ or $\sigma_{n\theta}$ and $\sigma_{\theta s} = 0$ (axisymmetry).

6.4. On DE or down stream exit condition

$\sigma_{zz}^* = 0$ or $\sigma_{zz} = 0$,

$$v_r^* = v_\theta^* = 0 \quad \text{or} \quad v_r = v_\theta = 0.$$

6.5. On BE or center symmetry line

$$v_r^* = v_\theta^* = 0 \quad \text{or} \quad v_r = v_\theta = 0,$$

$$\sigma_{rz}^* = 0 \quad \text{or} \quad \sigma_{rz} = 0 \qquad \text{(no shear stress)}.$$

At point C there is a stress singularity. At this point there is a sudden change in boundary condition, from no-slip to free-surface flow. This introduces some difficulties which will be addressed in the next section.

7. EVALUATION AND VALUES OF THE NSDs

The functional dependence between the NSDs' numbers and $\dot{\gamma}^*$ is expressed by

$$\text{NSD}_1 = \frac{a_1}{1 + b_1 d^2}, \qquad \text{NSD}_2 = \frac{a_2}{1 + b_2 d^2}, \tag{15}$$

where $d^2 = \frac{1}{2} d_{ij} d_{ij}$ and d_{ij} is the rate of the deformation tensor, and a_1, b_1, a_2, and b_2 are constants.

As discussed before, there is an important controversy in the literature about the proper signs of the NSDs for 'physically realistic fluids'. Aside from the work of Dunn and Rajagopal [12] which has been discussed before, Coleman and Markovitz [9] concluded that NSD_1 should be negative whenever Equation (4) occurs as an expansion of some special constitutive equations to terms of second-order in a retardation parameter. This is the same conclusion found experimentally by Markovitz and Brown [8] and by Tanner [21] using a poly-isobutylene–cetane solution. However, work performed by Ting [7] on unsteady flows, and work by Coleman *et al.* [10] on laminar shearing flow, pointed to instability and non-existent results when NSD_1 is negative. Others [22–24] argue that the sign of NSD_1 is a function of shear rate.

The results presented here take no side on the above issue. Some of the results presented are anticipated below, by saying that numerical solutions for *both* positive and negative values of the constants a_1, b_1 (and in a few cases for a_2 and b_2) were found. Several values of the constants a_1, b_1, a_2, and b_2 were tested, although convergence was possible for only some of the values.

8. SOLUTION METHOD AND LIMITATIONS ON THE SIMULATION

The analysis presented here was based on Fidap, a commercial finite element software package. A numerical simulation was performed for a given set of conditions, as was a detailed analysis of the flow. However, only the swell was measured and is presented here. The value of the parameters that increase the swell are shown, up to the convergence limits of the numerical simulation. For certain simulations, there are quite often severe limitations on the range of results presented. In a paper that has some relevance to the problem here, Keuning [13] gives an overview of the difficulties associated with the solution of free-surface flows for the case of viscoelastic fluids. In general, these difficulties can be traced to the following particulars of the problem:

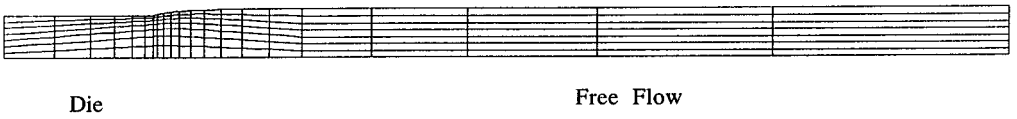

Figure 3. Schematic representation of the mesh for a straight die.

- Swell behavior involves a free-surface that is not known in advance and must become part of the solution.
- A stress singularity at point C in Figure 1 results in stresses becoming infinite at the die exit. In a numerical method, a given mesh size limits the magnitude of the stress, but with increasing mesh refinement this stress would increase without boundaries, which is an argument for selecting a moderate mesh size. Further work on the singularity of the stress at this point can be found in References [16,25–28].
- Finally, there are limitations that pertain to inherent instabilities that physically occur on the flow, which, if captured by the simulation, would explain why convergence cannot be attained.

9. PARTICULARS OF THE FINITE ELEMENT SOLUTION

The phenomenon of die swell is produced by relaxation of the velocity profile and stress fields from the values inside the die to a uniform velocity profile and isotropic stress field of the free jet. The relaxation of variables is balanced by viscous forces in the fluid. Other forces such as surface tension and gravity are neglected (both set to zero) in the simulation. Because the problem is highly non-linear, it is solved in two stages. The flow is first solved for an inlet boundary condition (parabolic velocity distribution on line AB in Figure 1), which is one-tenth of the final condition. The simulation is performed with the free-surface modeled in an immobile boundary condition. Then the solution to this simulation is used as the starting point of a simulation with an actual free-surface condition. The inlet boundary condition is then incremented 10 times by using the result of the previous solution as the starting point of the following solution, until the desired velocity values at the entrance to the die are reached.

As for other boundary conditions, the solution sets point C as fixed in space, although the angle of the free boundary at this point is set free. The slope at point D is set to zero, although its vertical position is free and determined by the solution. The Newton–Rapson iterative method is used to solve the system of equations at each step. Other details can be found in the Fidap documentation manual [29].

The basic schematic representation of the mesh generated for a straight tubular die geometry is shown in Figure 3. For clarity, this mesh only shows one-half of the actual divisions used. Grid density was increased near the die exit, near the walls, and near the free-surface to better capture the velocity changes. The upstream distance from the die exit is 3.5 half-diameters, and the velocity profile specified at the die entry is parabolic (fully developed). The downstream distance is set to 20 half-diameters, which guarantees that the velocity vector at point D is horizontal. In all simulations, there were 645 nodal points, 203 elements, and 1651 unknowns (equations).

10. RESULTS AND DISCUSSION

Among the changes in the geometry of the die, several angles for a converging and diverging die should be considered. Finally, a half-converging half-tubular die is modeled. Several flow rates are considered for each geometry, along with changes in the values of the Reynolds number and values of the NSD_1 and NSD_2 numbers.

The displayed values represent those for which convergence was achieved. It might be possible to attain convergence for other values presented here, but that would be by an unforeseen manipulation of relaxation parameters that control the numerical method, or by some strategy other than the one explained in the previous section. These limitations must be seen within the context of a general lack of basic understanding of the pathology of loss of convergence (these problems are vividly clear in viscoelastic flow [26]).

10.1. Straight tubular die

We take the base case as that in which the velocity distribution at the die entrance is

$$V(r) = 2(1 - r^2), \quad 1/Re = 1.0,$$

$$a_1 = 0.333, \quad \text{and} \quad b_1 = a_2 = b_2 = 0 \quad \text{(from Equation (15))}. \tag{16}$$

The measured value of the die swell value was $B = 1.1334$, or 13.34%.

10.1.1. Variation with a_1 values. Several positive and negative values of a_1 where selected. Figure 4 illustrates the results. We can observe that, although there are solutions for positive and negative values of a_1, larger (positive) values of a_1 would result in greater die swell.

10.1.2. Variation with $1/Re$. Results of this simulation are presented in Figure 5. At smaller values of $1/Re$, there was no convergence. The percentage die swell displays an essentially logarithmic dependence on $1/Re$. Although the values of B are within a narrow range, the curve shows physically correct behavior, where, at very low values of $1/Re$, the material would swell without boundaries.

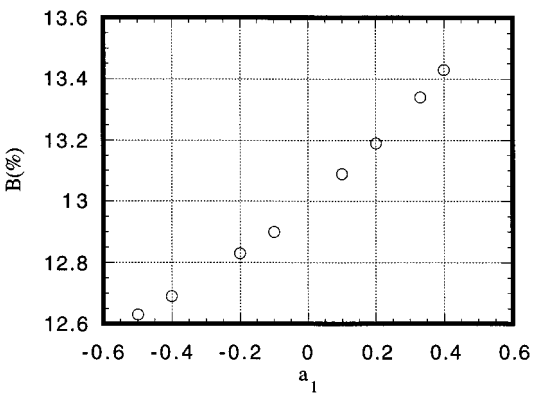

Figure 4. Die swell vs. a_1.

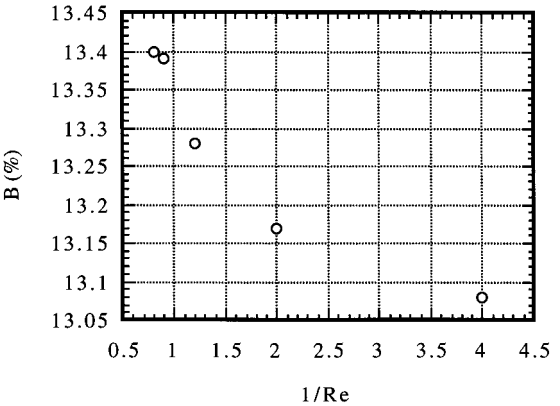

Figure 5. Die swell vs. $1/Re$.

10.1.3. Variations with mass flow rate. All variations with mass flow rate were accomplished by changing V in Equation (14). Two sets of points are shown, for positive and negative values of a_1. The results are shown in Figure 6.

It is interesting to note the different slopes of the trends of the two sets of points. In both cases, these trends seem to be linear, but again, the value of the swell did not change much as the velocity increased threefold. Similar qualitative results, for positive values of a_1, are presented in the literature for this same die geometry but for different solution schemes and fluid properties, e.g. by Luo and Tanner [30]. No convergence was possible for higher values of V, perhaps because instabilities were present in the flow. For positive values of a_1, the increasing trend seems to be physically correct, in as much as higher flow rates generate greater shearing at the die surfaces and should result in greater swell as the material exits the die. A similar argument also applies for negative values of a_1, where it can be argued that the shearing would result in negative normal stress that would yield a decreasing die swell.

In the cases that result in larger swell, i.e. on positive values of a_1, it was observed that even higher values were obtained for swell as mass flow rate was increased, but at greater values of normal stress coefficients. When the value of V is increased (from $V=2$ in the base case), and for $a_1 = b_1 = 1.9$, it was observed that the solution reaches a plateau, as shown in Figure 7.

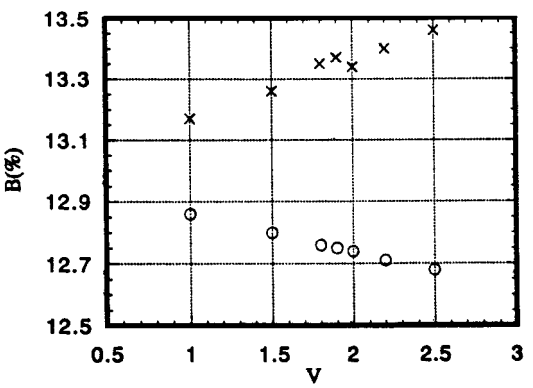

Figure 6. Die swell vs. V; $\times$, $a_1 = 0.333$, $\bigcirc$, $a_1 = -0.333$.

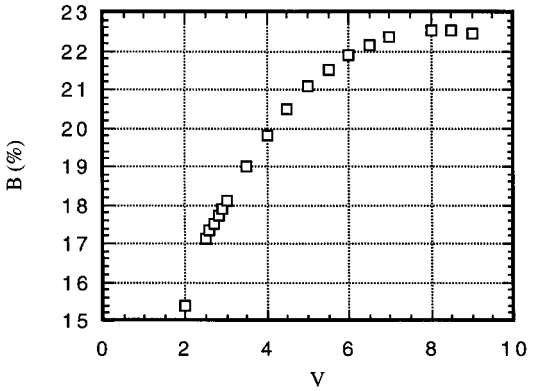

Figure 7. Die swell vs. V where $a_1 = b_1 = 1.9$.

Increasing the mass flow rate and the values of a_1 and b_1 allowed a simulation to be run with values of $a_1 = b_1 = 2.0$, $V = 8.6$ (all other parameters were as in the base problem) and the measured value of $B = 22.87\%$.

10.1.4. Variation with normal stress dimensionless numbers (NSDs). Variation with the constants a_1, b_1, a_2, b_2 of Equation (15) are more difficult to quantify and demonstrate. However, some general conclusions can be discussed before tabular results are presented.

All non-zero values of the second normal stress coefficients (a_2 and b_2) resulted in a diverging result when the first normal stress coefficients (a_1 and b_1) were not zero and positive. A few results could be obtained when a_1 and b_1 were zero, and when a_2 or b_2 were small. The maximum value of the swell, $B = 13.9\%$, was observed for $a_1 = b_1 = 0$, $a_2 = b_2 = 0.4$. For some values of a_1 negative, a few converged solutions can be obtained. Some samples are the following,

a_1	b_1	a_2	b_2	$B(\%)$
-0.1	0	0.4	0.4	13.82
-0.2	0	0.4	0.4	13.73

Larger values of swell were observed for non-zero values of a_1 and b_1 and when $a_2 = b_2 = 0$. When this was the case, and between a_1 and b_1, a_1 was observed to have a dominant effect on swell. Some examples of the above cases are shown in Table I.

10.1.5. Variation with $1/Re$ and with NSD_1. With these results in mind, a diagram of the die swell versus the normal stress coefficients is presented, where $a_1 = b_1$ has been taken, and for various values of the inverse of the Reynolds number ($1/Re$). Figure 8 shows that for $1/Re = 0.8$, the few obtained values suggest a curve similar to that corresponding to $1/Re = 1.0$, but displayed upward, as one would expect when viscous effects are less important in the flow. The opposite can be observed for $1/Re = 1.2$, where we can now obtain converged solutions for higher values of the normal stress parameters. No converged solutions were found for negative values of the horizontal axis.

Table I. Swell (%) vs. normal stress dimensionless parameter

		a_1				
		-1.0	-0.5	0.5	0.6	1.9
	0.2	12.35	12.62	13.55	13.70	
	0.4	12.32	12.61	13.55	13.69	
b_1	0.6	12.29	12.60	13.55	13.69	
	0.8	12.27	12.58	13.55	13.69	
	0.9			13.55		
	1.0				13.69	
	1.9					16.12
	2.0					16.10
b_1	2.1					16.08
	2.5					16.01
	3.0					15.94

10.2. Converging and diverging dies

It is of practical interest to quantify the variations in swell for various other geometries of the die. In converging and diverging dies, an extensional flow is superimposed on a shearing flow. Results from converging and diverging dies for Newtonian flows are discussed in References [31,32]. For the same mass flow rate as that of the base case (Equation (16)), the angle of the die is defined, as shown in Figure 9.

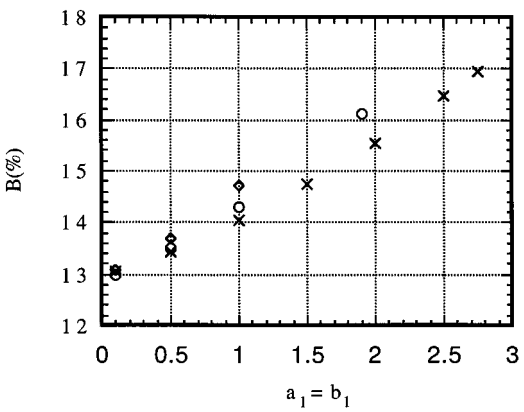

Figure 8. Die swell vs. $a_1 = b_1$; $\diamond$ $1/Re = 0.8$, $\circ$ $1/Re = 1.0$, $\times$ $1/Re = 1.2$.

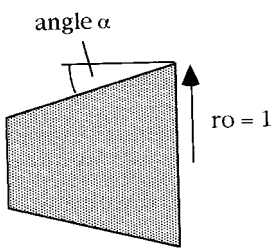

Figure 9. Angle α of the die used in the simulation.

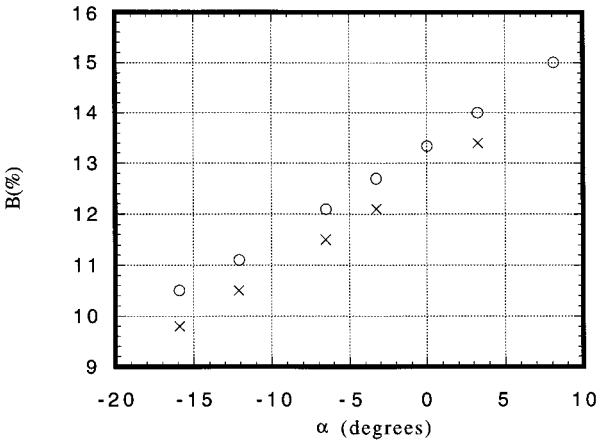

Figure 10. Die swell vs. angle α; ○ $a_1 = 0.33$, × $a_1 = -0.33$.

Plotting die swell as a function of the angle α produces the results shown in Figure 10, for $a_1 = \pm 0.33$. The die swell indicates an almost linear behavior with respect to the angle α for the range of values considered, where positive values in the variable a_1 produce more swell.

This is an unusual result, because for many fluids, contraction of the flow would result in greater swell (e.g. the work reported in Reference [33] on annular flows). Those results would seem to suggest that the die swell observed on such cases is due to stress relaxation as in viscoelastic materials. The results observed here would then be particular to our model.

10.3. Converging tubular die

A simplified geometry of a more complex and more realistic die geometry is shown in Figure 11. A similar geometry and a conceptually similar approach to this problem can be found in Reference [30], where some die swell results are presented as a function of the length of the tubular section. In the simulation of this paper, the geometry of the die is fixed with the proportions shown in Figure 11. A velocity vector diagram of a converged solution for this geometry is shown in Figure 12.

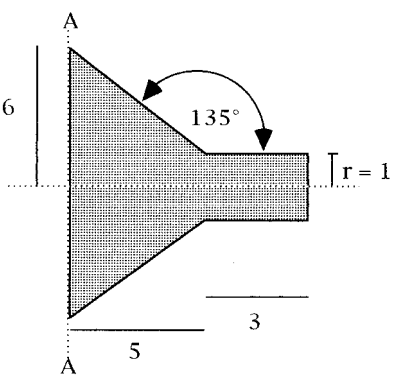

Figure 11. Simplified geometry of die used in the simulation.

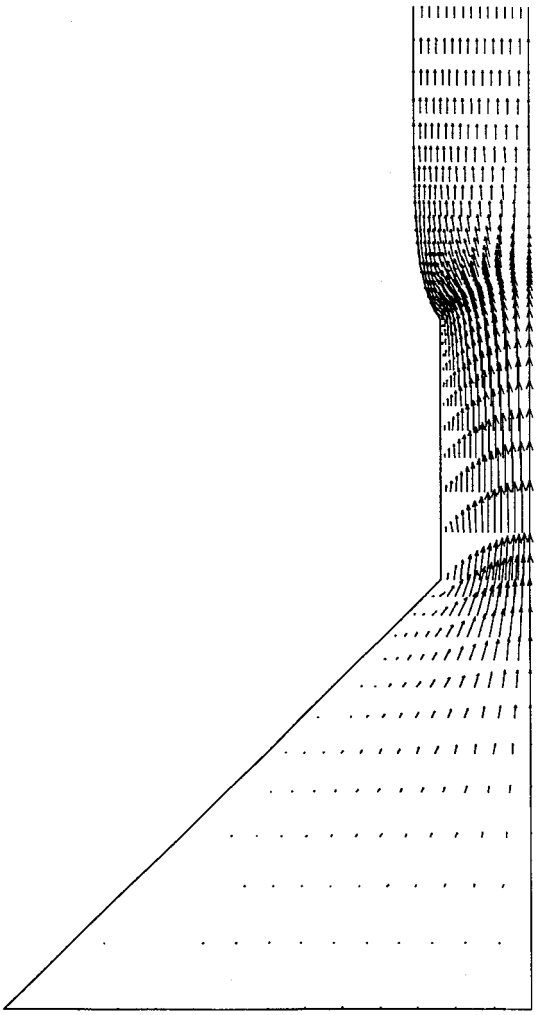

Figure 12. Diagram of velocity vectors when $V = 0.2$ and $a_1 = b_1 = 3.0$.

To establish a base case for our next series of simulations the following properties and parameters were set

$$1/Re = 1.0,$$

$$a_1 = b_1 = 2.0,$$

$$a_2 = b_2 = 0,$$

at section AA in Figure 11, $V(r) = 0.046(1 - r^2)$. This velocity distribution would be equivalent to a velocity distribution in the straight tubular section $V(r) = 1.6496(1 - r^2)$ if the converging portion was not present.

10.3.1. Variations with a_1. Figure 13 illustrates the variation of the die swell with a_1.

It is surprising to see that the die swell is almost constant for negative values of a_1; it is as if the swell had reached a minimum value and further changes in the properties of the material will no longer modify it. For positive values, the swell is directly dependent on the value of a_1.

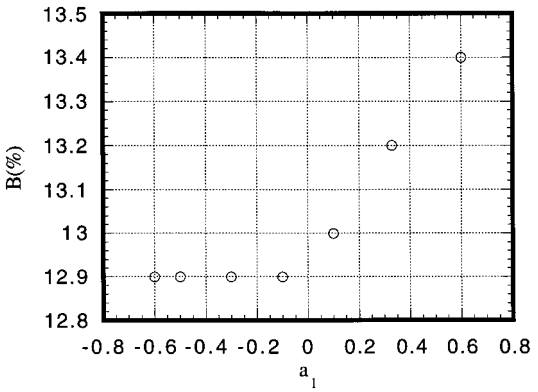

Figure 13. Die swell vs. a_1.

10.3.2. Variations with $1/Re$ and with the NSD_1. Results of a simulation in this geometry are presented in Figure 14, which displays die swell behavior versus the first normal stress coefficient and for three values of $1/Re$. As observed before in the case of straight tubular die, and for $1/Re = 0.8$, the few obtained values suggest a curve similar to that corresponding to $1/Re = 1.0$, but displayed upward, as one would expect for less viscous flow. A curve displayed downward was observed for $1/Re = 1.2$. When these results are compared with those obtained for a straight tubular die, it is observed from Table I that for $a_1 = b_1 = 1.9$, swell was 16.12%. This swell value is higher than that observed in Figure 14 for a smaller mass flow rate and a similar value of the first normal stress ($\approx 15.2\%$). This geometry, however, allows for solutions with greater values of the first normal stress coefficient, and, as the values of a_1 and b_1 increase, swell increases accordingly. No converged solutions were found for negative values of the horizontal axis.

10.3.3. Variation with flow rate. The centerline velocity V (set at $V = 0.046$ at the die entrance) was varied and the effect on the die swell was recorded. The variations are shown in Figure 15, where the maximum value of B is 24.1%, corresponding to an entry centerline velocity of $V = 0.2$.

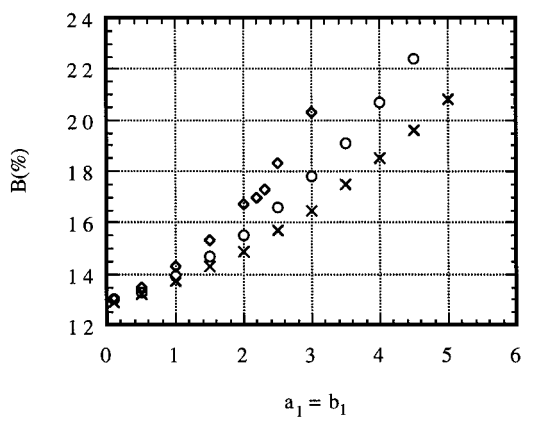

Figure 14. Die swell vs. $a_1 = b_1$; $\diamond$ $1/Re = 0.8$, $\circ$ $1/Re = 1.0$, $\times$ $1/Re = 1.2$.

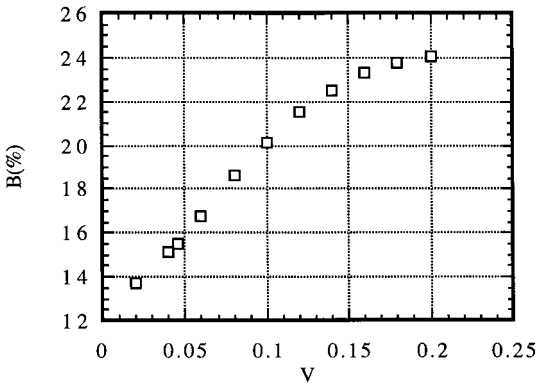

Figure 15. Die swell vs. inlet velocity V; $a_1 = b_1 = 2.0$.

One run was attempted with these same conditions but with $a_1 = b_1 = 3.0$; maximum swell was 29.2%.

11. CONCLUSIONS

Swell in this paper's model is a complex function of both the shear and unfolding deformation of the fluid. Solutions were found for positive and negative values of the normal stress coefficient. The influence of the second normal stress coefficient, for those few converged solutions obtained, seems to indicate that its effect on the swell appears to be of minor importance. Swell was strongly dependent on the first normal stress coefficient, and although solutions were found for both positive and negative values of the coefficient, positive values of the parameter a_1, were observed to have the stronger effect on the swell.

With respect to the numerical simulation, the complex interrelation of the flow conditions and the material properties on the process would preclude solutions in what sometimes seem simple extensions of past solutions. As with all numerical simulations, there is always great interest in discerning whether the limitations in obtaining a solution to a problem are due to the physics of the problem (instabilities) or to numerical difficulties. This question must be answered by experimentation.

ACKNOWLEDGMENTS

This work was supported by the Argonne National Laboratory, Energy Technology Division and Division of Educational Programs/Faculty Research Participation Program. The authors appreciate the assistance provided by Bob Noel, by Joseph Lucas and Chris Marshal during the developmental stages of this project, the support provided by Linda Washington, and that of the Reactor Engineering Division, in particular that of Theodore Bauer and James Morman.

REFERENCES

1. I.R. Tanner, *Engineering Rheology*, Oxford University Press, New York, 1985.
2. W.O. Criminale, J.L. Ericksen and G.L. Filbey, 'Steady shear flow of non-Newtonian fluids', *Arch. Ration. Mech. Anal.*, **1**, 410–417 (1957–1958).

3. B.D. Coleman and W. Noll, 'An approximation theorem for functionals, with applications in continuum mechanics', *Arch. Ration. Mech. Anal.*, **6**, 355–370 (1960).
4. C. Truesdell and W. Noll, *The Non-Linear Field Theories of Mechanics*, *Flügge's Hanbuch der Physik*, *III*, Springer, Berlin, 1965.
5. D.D. Joseph, 'Instability of the rest state of fluids of arbitrary grade greater than one', *Arch. Ration. Mech. Anal.*, **75**, 251–256 (1980–1981).
6. D.D. Joseph, *Fluid Dynamics of Viscoelastic Liquids*, Springer, Berlin, 1990.
7. T.W. Ting, 'Certain non-steady flows of second-order fluids', *Arch. Ration. Mech. Anal.*, **14**, 1–26 (1963).
8. H. Markovitz and D.R. Brown, 'Parallel plate and cone-plate normal stress measurements on poly(isobutylene)–cetane solutions', *Trans. Soc. Rheol.*, **7**, 137–154 (1963).
9. B.D. Coleman and H. Markovitz, 'Special section on high-polymer physics', *J. Appl. Phys.*, **35**, 1–9 (1964).
10. B.D. Coleman, R.J. Duffin and V. Mizel, 'Instability, uniqueness, and non-existence theorems for the equation $u_t = u_{xx} - u_{xtx}$ on a strip', *Arch. Ration. Mech. Anal.*, **19**, 100–116 (1965).
11. J.E. Dunn and R.L. Fosdick, 'Thermodynamics, stability, and boundedness of fluids of complexity 2 and fluids of second grade', *Arch. Ration. Mech. Anal.*, **56**, 191–272 (1974).
12. J.E. Dunn and K.R. Rajagopal, 'Fluids of differential type: critical review and thermodynamic analysis', *Int. J. Eng. Sci.*, **33**, 689–729 (1995).
13. R. Keunings, in C.L. Tucker III (ed), *Fundamentals of Computer Modeling for Polymer Processing*., Hanser-Gardner, Cincinnati, 1989.
14. G. Barakos and E. Mitsoulis, 'Non-isothermal viscoelastic simulations of extrusion through dies and prediction of the bending phenomenon', *J. Non-Newton. Fluid Mech.*, **62**, 55–79 (1996).
15. Y. Ahn and M. Ryan, 'Analysis of extrudate swell from an annular die', *Comput. Fluids*, **21**, 267–289 (1992).
16. G. Georgious, W. Schultz and L. Olson, 'Singular finite elements for the sudden-expansion and the die-swell problems', *Int. j. numer. methods fluids*, **10**, 357–372 (1990).
17. P. Hurez, P. Tanguy and F. Bertrand, 'A finite element analysis of the die swell with pseudoplastic and viscoplastic fluids', *Comput. Methods Appl. Mech. Eng.*, **86**, 87–103 (1991).
18. H. Giesekus, 'The simultaneous translations and rotational motion of a sphere in an elasticoviscous fluid', *Rheol. Acta*, **1**, 59–71 (1963) (in German).
19. R.I. Tanner and A.C. Pipkin, 'Intrinsic errors in pressure-hole measurements', *Trans. Soc. Rheol.*, **13**, 471–484 (1969).
20. A.C. Pipkin, 'Small finite deformations of viscoelastic solids', *Rev. Mod. Phys.*, **36**, 1034–1041 (1964).
21. R.I. Tanner, 'Methods for estimating the normal stress functions in viscometric flows', *Trans. Soc. Rheol.*, **14**, 483–507 (1970).
22. G. Kiss and R.S. Porter, 'Rheology of concentrated solutions of helical polypeptides', *J. Polysacch. Phys.*, **18**, 361–388 (1980).
23. K.K. Lem and C.D. Han, 'Rheological behavior of concentrated suspensions of particulates in unsaturated polyesater resin', *J. Rheol.*, **27**, 263–288 (1983).
24. A.D. Gotsis and D.G. Baird, 'Primary normal-stress difference for two liquid-crystalline copolyesters', *Rheol. Acta*, **25**, 275–286 (1986).
25. S. Richardson, 'The die swell phenomena', *Rheol. Acta.*, **9**, 193–199 (1970).
26. M. Crochet, 'Numerical simulation of viscoelastic flow. A review.', *Rubber Chem. Technol.*, **62**, 426–455 (1989).
27. W. Schultz and C. Gervasio, 'A study of the singularity in the die swell problem', *J. Mech. Appl. Math.*, **43**, 407–425 (1990).
28. T. Salamon, D. Bornside, R. Armstrong and R. Brown, 'The role of surface tension in the dominant balance in the die swell singularity', *Phys. Fluids*, **7**, 2328–2344 (1995).
29. Fidap Manuals. Fluid Dynamics International, Evanston, IL, 1995.
30. X.L. Luo and R.L. Tanner, 'Finite element simulation of long and short circular die extrusion experiments using integral models', *Int. j. numer. methods eng.*, **25**, 9–22 (1988).
31. M.J. Crochet and R. Keunings, 'Numerical simulation of die swell: geometrical effects', *Proc. 2nd World Cong. on Chemical Engineering*, 6, 285, C.S.Ch.E., Montreal, (1981).
32. W. Allan, 'Newtonian die swell evaluation for axisimmetric tube exits using a finite element method', *Int. j. numer. methods eng.*, **11**, 1621–1632 (1977).
33. A. Garcia-Rejon, R.W. DiRaddo and M.E. Ryan, 'Effects of die geometry and flow characteristics on viscoelastic annular swell', *J. Non-Newton. Fluid Mech.*, **60**, 107–128 (1995).

